DOI:
10.1148/radiol.2016150852

Document Version
Peer reviewed version

Title: Whole-brain diffusion MRI tractography reveals abnormal microanatomical fibre structures in patients with nodular heterotopia

Advances in knowledge:

1. Whole-brain Constrained Spherical Deconvolution (CSD) based fibre tractography and super-resolution Track Density Imaging (TDI) mapping revealed abnormal fibre projections in nodular tissue suggestive of abnormal organization of white matter (with abnormal fibres both within nodules and projecting to the surrounding white matter) in patients with bilateral periventricular nodular heterotopia (PVNH).
2. The detection of abnormal fibre structures by all four readers in all fourteen patients studied (Fleiss Kappa (κ) = 1.0 SE = 0.0, 95% CI = 1.0 to 1), indicates that these architectural abnormalities are particularly prevalent in patients with bilateral PVNH.

Implications for patient care:

Whole-brain tractography mapping techniques provide an opportunity to non-invasively detect *in vivo* abnormal structures potentially involved in ictal networks; such maps could be used to aid the identification of appropriate surgical targets for individuals undergoing evaluation for epilepsy surgery.

Summary statement:

Whole brain CSD based tractography and TDI maps reveal the presence of abnormal fibre tracks projecting from heterotopic nodules in patients with PVNH that are not detected with conventional neuroimaging techniques routinely used to investigate malformations of cortical development *in vivo*.

Abstract

Purpose: In this study, we use whole-brain Constrained Spherical Deconvolution (CSD)-based fibre tractography and super resolution Track Density Imaging (TDI) mapping to investigate whether it is possible in patients with periventricular nodular heterotopia (PVNH) to detect abnormal fibre projections that have only previously been reported in the histopathological literature.

Methods: Whole-brain DWI data from fourteen patients with bilateral PVNH and fourteen age/sex matched controls were prospectively acquired using 3T MRI between 01/08/2008-05/12/2012. All participants provided prior written informed consent. The DWI data were processed using the MRtrix software package to generate whole-brain CSD-based tractography and TDI maps. The tractography results were overlaid on co-registered 3D T1 weighted images to visually assess regions of heterotopia. A panel of MRI researchers independently assessed each case, and indicated numerically (No = 1 / Yes = 2) as to the presence of abnormal fibre tracks in nodular tissue. The Fleiss Kappa statistical measure was applied to assess the reader agreement.

Results: Abnormal fibre tracks emanating from one or more regions of heterotopia were reported by all four readers in all 14 patients with PVNH studied (Fleiss Kappa (κ) = 1). These abnormal structures were not visible in the tractography data of any of the control subjects, and not discernable on the conventional T1 weighted images of the PVNH patients.

Conclusion: Whole-brain CSD-based fibre tractography and super-resolution TDI mapping reveals abnormal fibre projections in nodular tissue suggestive of abnormal organization of white matter (with abnormal fibres both within nodules and projecting to the surrounding white matter) in patients with bilateral PVNH.

Introduction

Malformations of cortical development (MCD) have been the subject of much interest in recent years due to the insight they provide into human cerebral development (1,2). In some cases there is a known genetic association (e.g. mutations in the *Filamin A* (*FLNA*) gene (3–6), while in many cases there is no known cause. Individuals with neuronal migration disorders where an arrest in the migration of neurons results in collections of normal neurons in abnormal locations, such as in periventricular nodular heterotopia (PVNH), often present with epilepsy that is refractory to medical and surgical treatment (1,7,8). Although the signal characteristics of heterotopic nodules appear similar to that of normal grey matter when using conventional MRI techniques, there is histological evidence to suggest that some nodules have linear bundles of myelinated fibres emanating from within the nodular nest (9). These histopathological features are important because they provide a structural basis for the complex interaction between epileptogenic nodular tissue and overlying cortex, such as that described in functional studies of heterotopia patients with epilepsy (10–12).

Advances in MRI Diffusion-Weighted Imaging (DWI) analysis methods now provide an opportunity to investigate the consequences of abnormal cerebral development beyond those apparent on conventional structural MRI. In particular, High Angular Resolution Diffusion Imaging (HARDI) analysis methods have been developed specifically to provide robust estimates of fibre orientations within voxels (13–17), and provide more reliable delineations of white matter pathways throughout the brain than previously possible using Diffusion Tensor Imaging (DTI) based techniques (18). These advances have also more recently led to the development of novel high-contrast super-resolution imaging techniques such as Track Density Imaging (TDI) (19,20). TDI exploits the distributed information obtained from streamlines generated by performing whole brain tractography to achieve high contrast images at spatial resolutions far beyond that at which the data were originally acquired (19).

In this study, we use whole-brain Constrained Spherical Deconvolution (CSD)-based fibre tractography (21,22) and super resolution Track Density Imaging (TDI) (19,20) mapping to investigate whether it is possible in patients with periventricular nodular heterotopia (PVNH) to detect abnormal fibre projections that have only previously been reported in the histopathological literature (9).

Materials and Methods

The authors AC, GJ, FC & J-DT, declare a patent application related to track density imaging methods used in this work. The data were analysed by SM (Neuroradiologist - 20 years' experience), GJ (Neurologist - >30 years' experience), AC (MRI physicist - >30 years' experience), and SF (MRI Radiographer - 20 years' experience). SF was also responsible for the processin*g* of all data.

Study Participants

A consecutive series of fourteen patients were prospectively recruited to this study between August 2008 and December 2012. Patients were invited to take part in the study if they had prior neuroimaging confirming the presence of bilateral PVNH at the time of presentation to the referring Neurologist, and included in the study if they were able to adequately undertake a research 3T Magnetic Resonance Imaging (MRI) at the Melbourne Brain Centre, Florey Institute of Neurosciences and Mental Health, Melbourne Australia. The patients' mean age was 36 years, (age range: 4 months - 68 years, SD 18 years), 4 male: 10 female, including 7 *Filamin* A (*FLNA*) positive females. The mean age of the four male patients was 34 (age range: 30 - 39 years), and the mean age for the ten female patients was 37 (age range: 4 months - 68years). Table 1 shows MRI findings, epilepsy and *FLNA* mutational status. (Note: details of mutation and clinical descriptions of members of Family B, with the exception of the infant (patient 14), and functional MRI data from patient 11, have previously been published (3,23,24, and 12 respectively). Fourteen control individuals matched for sex and age were recruited to this study. All participants were recruitedin accordance with procedures approved by the Austin Health Human Research Ethics Committee, Melbourne, Australia. All participants provided written informed consent prior to participation. Subjects were to be excluded from the study if they were unable to adequately complete the research MRI scan; however, all subjects recruited successfully completed the additional research MRI scan, so none was excluded.

Data Acquisition

Magnetic resonance imaging data were acquired on a 3T Siemens TIM Trio MRI system with a 12-channel receive-only head coil. Axial diffusion-weighted data were obtained for all patients and healthy controls using a twice-refocused single shot echo-planar imaging sequence, with 60 diffusion weighted directions uniformly distributed over a hemisphere in a scan time of 9.5 minutes (44 slices acquired interleaved, FOV 240 × 240 mm^2, matrix size 96 × 96, voxel size 2.5mm isotropic; b = 3000 sec/mm^2, TE 110 msec, TR 8400 msec, parallel acceleration factor (iPAT) 2). For all participants, additional high-resolution T1-weighted (3D MPRAGE) data were also acquired for anatomical reference.

Data processing

Diffusion-weighted imaging (DWI) data were processed on a Linux workstation using the MRtrix software package for diffusion MRI analysis (22). The high *b*-value diffusion data were first corrected for motion by aligning all DWI volumes to the mean whole-brain brain mask (22). The motion corrected DWI data were then processed using a neighbourhood regularised version (25) of CSD (21,22) with a maximum spherical harmonic degree l_{max}= 8, to estimate fibre orientation distributions (FOD) within each imaging voxel of a whole-brain mask generated for each individual based on the *b*=0 image.

Whole-brain CSD-based tractography mapping

We used a 'whole-brain' tractography approach, whereby tracks are initiated from seed points randomly distributed throughout the white matter to track throughout the whole-brain mask in each individual's own space. Fibre tracking was performed on each DWI data set using the 2nd order integration over fibre orientation distributions (iFOD2) (26) probabilistic streamlines algorithm implemented in MRtrix (22). In each case, a tractogram of 1 million tracks (i.e. streamlines) was generated by randomly seeding points throughout the white matter in each individual's own space. Tracks were propagated in both directions from all voxels within the white matter using a step size = 1.25 mm, a maximum angle between steps = 45°, and a minimum

track length = 5 mm, and tracking was terminated if the FOD amplitude termination threshold = <0.1 was reached. For display purposes, an additional tractogram was also generated with 100,000 tracks for each participant using the exact same processing constraints. From a technical perspective, this whole brain tractography approach allowed us to avoid potential sources of error inherent in 'seed to target' region-of-interest-based tractography approaches where assessment of structural connectivity, and comparison to control subjects, is complicated by the absence in control subjects of structures corresponding to the ectopic clusters of neurons (27–32). (This potential source of error is particularly important in cases where abnormal connections are suspected, and also in cases where imaging data and analysis methods are susceptible to partial volume effects due to image acquisition constraints.) The CSD-based tractography results were colour coded according to track orientation (red: left to right, green: anterior-posterior, blue: inferior-superior).

Super-resolution TDI maps

The super-resolution TDI maps (19,20) were generated from the whole-brain CSD tractography maps (21) by calculating the total number of tracks present in each element of a 0.5mm isotropic grid using the technique described by Calamante et al., 2010 (19,20), and default values from MRtrix (22). Tracks less than 5mm were excluded from TDI calculations to ensure that only tracks consistent with the local neighbourhood contributed to the track-density value in each grid element. The sum of tracks traversing each 500x500x500μm^3 voxel defines the resultant intensities displayed in the super resolution TDI greyscale and heat-scale maps (19,20). The directionally-encoded colour (DEC) TDI maps were generated by also assigning an RGB colour to each spatial direction (red: left to right, green: anterior-posterior, blue: inferior-superior), and averaging the colours of all streamline segments contained within each 500x500x500μm^3 grid element. The resultant the DEC-TDI maps display the main local orientation of all the streamlines contained within each grid element whilst maintaining the super resolution characteristics inherent to TDI (19,20). (See figure 1 for an example, in a control participant, of the improved spatial

resolution, high contrast to noise ratio (CNR) and signal to noise ratio (SNR) inherent in TDI data at 500μm compared to the original DWI data acquired with 2.5mm isotropic voxels.)

Data analysis

The 3D T1-weighted anatomical images for each individual were coregistered and realigned individual's Fractional Anisotropy (FA) map using the rigid body co-registration function in SPM8 (http://www.fil.ion.ucl.ac.uk/spm/). The whole-brain CSD-based tractography results and TDI maps were then displayed overlaid on the coregistered 3D T1-weighted anatomical images, to aid the anatomical localisation of abnormal fibres within regions of heterotopia.

The results for all participants were assessed on a Linux workstation using the image viewer within MRtrix software (22) by a team of experienced MRI researchers that included: a Neuroradiologist (SM), Neurologist (GJ), MRI physicist (AC), and an MRI Radiographer (SF). The Neuroradiologist (SM) first reviewed the 3D T1-weighted data to identify the regions of heterotopia in each patient with bilateral PVNH. The whole brain CSD-based tractography (21,22) and TDI maps (19,20) for all participants were then overlaid on the coregistered 3D T1-weighted data by the MRI Radiographer (SF) to facilitate visual assessment of tractography results in the regions of heterotopia, and comparison of the patient results to the data from the age and sex matched healthy control. Each of the four readers (SM)(GJ)(AC)(SF) independently indicated numerically (No = 1, Yes = 2) for each patient whether abnormal fibre tracks were present in nodular tissue in both the whole brain CSD fibre tractography (21) and TDI maps (19). Fleiss Kappa was calculated to assess the agreement between the four readers as to the presence of abnormal fibre tracks in the fourteen patients with PVNH studied.

*Fleiss Kappa **(κ)**:*

$$\kappa = \frac{\bar{P} - \bar{P}_e}{1 - \bar{P}_e}$$

where;

$$\bar{P} = \frac{1}{Nn(n-1)}\left(\sum_{i=1}^{N}\sum_{j=1}^{k} n_{ij}^2 - Nn\right),$$

$$\bar{P_e} = \sum_{j=1}^{k}\left(\frac{1}{Nn}\sum_{i=1}^{N} n_{ij}\right),$$

N is the total number of subjects (subjects are indexed by *i*), *n* is the number of observers/readers, *k* is the number of categories (categories are indexed by *j*), and n_{ij} is the number of observers who rated the subject *i* in the *j*th category.

Results

Abnormal fibre tracks emanating from one or more regions of heterotopia were reported to be seen using whole brain fibre CSD-based tractography (21) and TDI maps (19) in all 14 patients with bilateral PVNH by all four raters in all of the patients with PVNH studied (Fleiss Kappa (κ) = 1.0 SE = 0.0, 95% CI = 1.0 to 1.0, based on N=14, n=4, k =2, $\sum_{i=1}^{N} n_{i1}$ = 0, $\sum_{i=1}^{N} n_{i2}$ = 56). These abnormal structures were not visible in the tractography data of any of the control subjects, and not discernable on the conventional T1 weighted images. Figures 2, 3(a-c), 4 and 5 show examples of whole-brain CSD-based tractography (21,22) results and TDI maps (19,20) from representative patients with PVNH.

Abnormal tracks were seen in all patients regardless of nodule load; however, in individual patients these abnormal structures were not visible in all clusters of nodules. The directionally colour-encoded images demonstrated that the orientation of these abnormal fibre tracks was not limited to a single direction. Figure 3 shows an example CSD-based tractography results from a PVNH patient with a cluster of nodules in the frontal lobe that superiorly displace the corpus callosum, from within which abnormal fibres can clearly be seen projecting laterally.

Bilateral symmetrical banks of nodules were observed on the T1 weighted data in all patients who had a *FLNA* mutation. In individual patients, abnormal fibre tracks were not observed in all clusters of nodules lining the ventricular wall. Figure 4 shows example TDI data from a family

with the *FLNA* mutation, a grandmother (68 years), mother (35 years) and daughter (4 months), all of whom have extensive banks of nodules lining the ventricular wall bilaterally (Figures 4(i)) within which abnormal fibre tracks can be observed emanating from some of the clusters of nodules (Figures 4(ii & iii)). Figure 5 shows the CSD-based tractography (21) data depicting abnormal fibres projecting from distinct clusters of nodules in the 4 month old female with the *FLNA* mutation (and also data from an age matched control participant). These data also collectively demonstrated the displacement of white matter pathways such as the corticospinal tracts and superior longitudinal fasciculus in cases where there are extensive banks of nodules lining the ventricular wall.

The abnormal fibre projections within clusters of nodules shown in this study appear consistent with bundles of myelinated fibres previously demonstrated using traditional histopathology. Figure 6 shows an example histological image (from Kakita et al., (9)) of heterotopic nodules containing linear bundles of myelinated fibres (blue arrows) from the brain tissue of a 48 year old *FLNA* positive female with bilateral PVNH) (9).

Discussion

In the current study, whole-brain CSD based fibre tractography (21,22) and super-resolution TDI (19,20) mapping reveal the presence of abnormal fibre tracks projecting from heterotopic nodules in all patients studied with bilateral Periventricular Nodular Heterotopia (PVNH). These abnormal structures were not visible in the tractography data of any of the control subjects, and not discernable on the conventional T1 weighted images. In individual patients these abnormal structures were not visible in all clusters of nodules lining the ventricular wall; and the directionally colour-encoded images demonstrated that the orientation of these abnormal fibre tracks was not limited to a single direction.

These microanatomical imaging features are important because there is discordance in the cytoarchitectural literature as to whether there is also abnormal organization of white matter pathways in patients with this disorder of neuronal migration. Initial histological and carbocyanine dye (DiI) tracing studies investigating brain tissue from children with subcortical or periventricular nodular heterotopia of different aetiologies suggest that, although there is some connectivity between adjacent nodules, there is limited evidence to suggest that there are connections projecting from nodules to the remainder of the brain (33). In contrast, Kakita et al., (2002) using similar techniques to study the brain tissue of a 48 year old female with a FLNA mutation, demonstrated widespread abnormal axonal connectivity with abnormal fibres projecting both between nodules and to the surrounding white matter (9). The differences in the DiI connectivity findings of these studies (9,33) suggest that the etiology of abnormal neuronal migration might be an important factor in determining whether and where there is also abnormal organization of white matter structures. The data presented in the present work provide additional imaging evidence suggestive of widespread abnormal organization of white matter (with abnormal fibres both within nodules and projecting to the surrounding white matter). There was unanimous agreement among four observers that abnormal tracks could be detected in all 14 patients with bilateral PVNH studied (the majority of whom presented without associated severe malformation

complexes, and half of whom had an identified genetic basis).

The ability to detect abnormal structures within regions of heterotopia using non-invasive whole-brain diffusion MRI tractography mapping techniques represents a radiological advance that carries important clinical implications. In patients with PVNH, approximately 80% develop epilepsy (34) that may be refractory to medical and surgical treatment (1,8). Intervention for those who undergo epilepsy surgery often relies on invasive intracranial recordings (35,36) to help identify which regions are involved in ictal networks in the context of many potentially epileptogenic sites. The functional literature suggests that the synchronization and amplification of abnormal neuronal activity might be subserved by a circuit of neuronal connections between nodules, and between nodules and cortex (11,12,37). The abnormal connections observed here, and in previous histopathology studies (9), provide a structural basis for this complex functional interaction between epileptogenic nodules and the rest of the brain.

This current work also illustrates how advanced imaging methods can deepen understanding of the structural phenotypes of genetic defects. Bilateral PVNH is often due to mutations in FLNA (3–6); however, in many cases and phenotypic subgroups of PVNH (38), the genetic aetiology is not known. Gross anatomical consequences on brain development that are a result of genetic mutations, are often readily visible on structural MRI. However, the more subtle aspects of the phenotype that may be present in addition to the gross anatomical changes, or in some cases the more subtle effects that may even constitute the sole phenotype, may be missed and require investigation using more sensitive techniques to provide insight into the biology of genetic defects. All of our seven FLNA positive patients showed abnormal fibres, including the youngest aged 4 months who was not experiencing seizures. In the three generations of her family, all three affected females had abnormal fibres tracks emanating from some regions of heterotopia within the extensive bilateral banks of nodules lining the ventricular wall. Interestingly, the whole-brain tractography results from the infant demonstrate particularly prominent abnormal fibre projections. These structures were not present in all nodules, and were not present in the matched

control infant. Since we can now detect such structures *in vivo*, it will be important to investigate how these architectural abnormalities change as the brain matures, particularly in cases where subjects are at risk of developing epilepsy in the future.

The findings presented in this work are an advance on previous diffusion tractography studies that utilise the Diffusion Tensor Imaging (DTI) model to provide estimations of fibre orientations from diffusion weighted data, despite it being well recognised to be fundamentally limited for this purpose (18). The DTI model is confounded by being unable to fit fibre orientation estimates correctly when there is more than one fibre within each voxel (present in >90% of white matter voxels) (39), leading to the generation of incorrect fibre orientation estimates. One manifestation of this problem is that when small fibre bundles and large fibre bundles are present in the same voxel, the estimated direction is biased towards the dominant fibre bundle, resulting in significantly reduced sensitivity when tracking non-dominant fibre populations (18,40). This problem is of particular concern for tractography studies of malformations of cortical development that are located on the ventricular surface, since these are adjacent to large fibre bundles such as the corticospinal tracts and the longitudinal fasciculus, which would lead to obscuration of subtle fibre projections when using DTI. To avoid the above DTI-related problems, we address this issue by utilising a HARDI-based analysis method, CSD (21,22), which was specifically developed to address the fundamental limitations of the DTI model. The advantage of the CSD model is that it provides robust fibre orientation estimations (14–17), even in voxels comprised of multiple fibre populations, allowing more reliable tract-based comparisons throughout the brain (21,22). Using this HARDI-based tractography method we detected discrete fibre tracks associated with PVNH despite the fact that they are in close vicinity of major fibre bundles.

A limitation of the tractography-based imaging techniques used in the present study is that, although they provide images that reveal anatomy that cannot be discerned using conventional anatomical MRI, it is well recognised that parameters such as ‘track counts’ cannot be used in their raw form as a quantitative metric (41). This is relevant to the present work in that Track

Density Imaging (TDI) does not provide a quantitative measure of white matter fibres (19,42). A number of recent novel methods in the technical literature can in principle facilitate quantitation of tractography streamlines (43–47); however, optimal use of such methods requires additional processing (48) to correct for track termination errors, and such processing requires reference data (to correct for image distortions) that are not available in this cohort of patients. An additional limitation of the work presented here is that it is difficult to rigorously delineate boundaries between clusters of nodules using MRI, especially in cases where there are contiguous nests of nodules lining the length of ventricular wall as observed in our patient cohort. This radiological limitation in nodule delineation means it is not possible to quantify the proportion of nodules in which abnormal structures can be seen. Finally, in order to relate the observed abnormal structures to seizure genesis, we would need to be able to precisely localise seizure origin and propagation. An important area of future research, therefore, will be to investigate the functional interaction between abnormal structures associated with some nodules and any epileptogenic nodules or related cortex.

In summary, **whole brain CSD based tractography and TDI maps reveal the presence of abnormal fibre tracks projecting from heterotopic nodules in patients with PVNH that are not detected with conventional neuroimaging techniques routinely used to investigate malformations of cortical development *in vivo*.** The ability to detect these architectural abnormalities *in vivo* represents a radiological advance that carries important clinical implications because these abnormal connections provide a structural basis for complex functional interactions, described in recent functional MRI studies, between epileptogenic nodules and the rest of the brain. Future research may provide valuable insight in to the pathophysiological mechanisms of epilepsy if we can establish the role that these abnormal structures have within ‘epileptogenic networks’.

References:

1. Barkovich AJ, Kjos BO. Gray matter heterotopias: MR characteristics and correlation with developmental and neurologic manifestations. Radiology. 1992;182:493–499.

2. Barkovich AJ, Guerrini R, Kuzniecky RI, Jackson GD, Dobyns WB. A developmental and genetic classification for malformations of cortical development: update 2012. Brain. 2012;135:1348–1369.

3. Eksioğlu YZ, Scheffer IE, Cardenas P, et al. Periventricular Heterotopia: An X-Linked Dominant Epilepsy Locus Causing Aberrant Cerebral Cortical Development. Neuron. 1996;16:77–87.

4. Fox JW, Lamperti ED, Ekşioğlu YZ, et al. Mutations in filamin 1 Prevent Migration of Cerebral Cortical Neurons in Human Periventricular Heterotopia. Neuron. 1998;21:1315–1325.

5. Sheen VL, Dixon PH, Fox JW, et al. Mutations in the X-linked filamin 1 gene cause periventricular nodular heterotopia in males as well as in females. Hum Mol Genet. 2001;10:1775–1783.

6. Guerrini R, Mei D, Sisodiya S, et al. Germline and mosaic mutations of FLN1 in men with periventricular heterotopia. Neurology. 2004;63:51–56.

7. Huttenlocher PR, Taravath S, Mojtahedi S. Periventricular heterotopia and epilepsy. Neurology. 1994;44:51–51.

8. Guerrini R, Carrozzo R. Epilepsy and genetic malformations of the cerebral cortex. Am J Med Genet. 2001;106:160–173.

9. Kakita A, Hayashi S, Moro F, et al. Bilateral periventricular nodular heterotopia due to filamin 1 gene mutation: widespread glomeruloid microvascular anomaly and dysplastic cytoarchitecture in the cerebral cortex. Acta Neuropathol (Berl). 2002;104:649–657.

10. Kothare SV, VanLandingham K, Armon C, Luther JS, Friedman A, Radtke RA. Seizure onset from periventricular nodular heterotopias: Depth-electrode study. Neurol Dec 1998. 1998;51:1723–1727.

11. Tyvaert L, Hawco C, Kobayashi E, LeVan P, Dubeau F, Gotman J. Different structures involved during ictal and interictal epileptic activity in malformations of cortical development: an EEG-fMRI study. Brain. 2008;131:2042–2060.

12. Archer JS, Abbott DF, Masterton RAJ, Palmer SM, Jackson GD. Functional MRI interactions between dysplastic nodules and overlying cortex in periventricular nodular heterotopia. Epilepsy Behav. 2010;19:631–634.

13. Tournier J-D, Mori S, Leemans A. Diffusion tensor imaging and beyond. Magn Reson Med. 2011;65:1532–1556.

14. Tournier J-D, Yeh C-H, Calamante F, Cho K-H, Connelly A, Lin C-P. Resolving crossing fibres using constrained spherical deconvolution: Validation using diffusion-weighted imaging phantom data. NeuroImage. 2008;42:617–625.

15. Moldrich RX, Pannek K, Hoch R, Rubenstein JL, Kurniawan ND, Richards LJ. Comparative mouse brain tractography of diffusion magnetic resonance imaging. NeuroImage. 2010;51:1027–1036.

16. Neher PF, Descoteaux M, Houde J-C, Stieltjes B, Maier-Hein KH. Strengths and weaknesses of state of the art fiber tractography pipelines – A comprehensive in-vivo and phantom evaluation study using Tractometer. Med Image Anal. 2015;26:287–305.

17. Wilkins B, Lee N, Gajawelli N, Law M, Leporé N. Fiber estimation and tractography in diffusion MRI: Development of simulated brain images and comparison of multi-fiber analysis methods at clinical b-values. NeuroImage. 2015;109:341–356.

18. Farquharson S, Tournier J-D, Calamante F, et al. White matter fiber tractography: why we

need to move beyond DTI. J Neurosurg. 2013;118:1367–1377.

19. Calamante F, Tournier J-D, Jackson GD, Connelly A. Track-density imaging (TDI): Super-resolution white matter imaging using whole-brain track-density mapping. NeuroImage. 2010;53:1233–1243.

20. Calamante F, Tournier J-D, Heidemann RM, Anwander A, Jackson GD, Connelly A. Track density imaging (TDI): Validation of super resolution property. NeuroImage. 2011;56:1259–1266.

21. Tournier J-D, Calamante F, Connelly A. Robust determination of the fibre orientation distribution in diffusion MRI: Non-negativity constrained super-resolved spherical deconvolution. NeuroImage. 2007;35:1459–1472.

22. Tournier J-D, Calamante F, Connelly A. MRtrix: Diffusion tractography in crossing fiber regions. Int J Imaging Syst Technol. 2012;22:53–66.

23. Poussaint TY, Fox JW, Dobyns WB, et al. Periventricular nodular heterotopia in patients with filamin-1 gene mutations: neuroimaging findings. Pediatr Radiol. 2000;30:748–755.

24. Sheen VL, Basel-Vanagaite L, Goodman JR, et al. Etiological heterogeneity of familial periventricular heterotopia and hydrocephalus. Brain Dev. 2004;26:326–334.

25. J-Donald Tournier, Calamante, Fernando, Connelly, Alan. A robust spherical deconvolution method for the analysis of low SNR or low angular resolution diffusion data. Proceedings of the ISMRM 21st Annual Meeting, Salt Lake City, Utah; 2013.

26. Tournier JD, Calamante F, Connelly A. Improved probabilistic streamlines tractography by 2nd order integration over fibre orientation distributions. Proc 18th Annu Meet Intl Soc Mag Reson MedISMRM. 2010. p. 1670

27. Eriksson SH, Symms MR, Rugg-Gunn FJ, et al. Exploring white matter tracts in band

heterotopia using diffusion tractography. Ann Neurol. 2002;52:327–334.

28. Lim CCT, Yin H, Loh NK, Chua VGE, Hui F, Barkovich AJ. Malformations of Cortical Development: High-Resolution MR and Diffusion Tensor Imaging of Fiber Tracts at 3T. Am J Neuroradiol. 2005;26:61–64.

29. Chang BS, Katzir T, Liu T, et al. A structural basis for reading fluency: White matter defects in a genetic brain malformation SYMBOL SYMBOL. Neurol Dec 4 2007. 2007;69:2146–2154.

30. Bonilha L, Halford J, Rorden C, et al. Microstructural white matter abnormalities in nodular heterotopia with overlying polymicrogyria. Seizure - Eur J Epilepsy. 2007;16:74–80.

31. Lu G, Zhang Z, Tan Q, et al. Disrupted Frontal Connections in Band Heterotopia Mapped by Diffusion Tensor Tractography. Clin Neuroradiol. 2008;18:231–236.

32. Christodoulou JA, Walker LM, Del Tufo SN, et al. Abnormal structural and functional brain connectivity in gray matter heterotopia. Epilepsia. 2012;53:1024–1032.

33. Hannan AJ, Servotte S, Katsnelson A, et al. Characterization of nodular neuronal heterotopia in children. Brain. 1999;122:219–238.

34. Dubeau F, Tampieri D, Lee N, et al. Periventricular and subcortical nodular heterotopia A study of 33 patients. Brain. 1995;118:1273–1287.

35. Aghakhani Y, Kinay D, Gotman J, et al. The role of periventricular nodular heterotopia in epileptogenesis. Brain. 2005;128:641–651.

36. Tassi L, Colombo N, Cossu M, et al. Electroclinical, MRI and neuropathological study of 10 patients with nodular heterotopia, with surgical outcomes. Brain. 2005;128:321–337.

37. Shafi MM, Vernet M, Klooster D, et al. Physiological consequences of abnormal connectivity in a developmental epilepsy: Cortical Connectivity. Ann Neurol. 2015;77:487–

503.

38. Mandelstam SA, Leventer RJ, Sandow A, et al. Bilateral Posterior Periventricular Nodular Heterotopia: A Recognizable Cortical Malformation with a Spectrum of Associated Brain Abnormalities. Am J Neuroradiol. 2013;34:432–438.

39. Jeurissen B, Leemans A, Tournier J-D, Jones DK, Sijbers J. Investigating the prevalence of complex fiber configurations in white matter tissue with diffusion magnetic resonance imaging: Prevalence of Multifiber Voxels in WM. Hum Brain Mapp. 2013;34:2747–2766.

40. Behrens TEJ, Berg HJ, Jbabdi S, Rushworth MFS, Woolrich MW. Probabilistic diffusion tractography with multiple fibre orientations: What can we gain? NeuroImage. 2007;34:144–155.

41. Jones DK, Knösche TR, Turner R. White matter integrity, fiber count, and other fallacies: The do's and don'ts of diffusion MRI. NeuroImage. 2013;73:239–254.

42. Calamante F, Smith RE, Tournier J-D, Raffelt D, Connelly A. Quantification of voxel-wise total fibre density: Investigating the problems associated with track-count mapping. NeuroImage. 2015;117:284–293.

43. Lemkaddem A, Skiöldebrand D, Dal Palú A, Thiran J-P, Daducci A. Global tractography with embedded anatomical priors for quantitative connectivity analysis. Front Neurol. 2014;5:1–13.

44. Pestilli F, Yeatman JD, Rokem A, Kay KN, Wandell BA. Evaluation and statistical inference for human connectomes. Nat Methods. 2014;11:1058–1063.

45. Daducci A, Dal Palu A, Lemkaddem A, Thiran J-P. COMMIT: Convex Optimization Modeling for Microstructure Informed Tractography. IEEE Trans Med Imaging. 2015;34:246–257.

46. Smith RE, Tournier J-D, Calamante F, Connelly A. SIFT: Spherical-deconvolution informed filtering of tractograms. NeuroImage. 2013;67:298–312.

47. Smith RE, Tournier J-D, Calamante F, Connelly A. SIFT2: Enabling dense quantitative assessment of brain white matter connectivity using streamlines tractography. NeuroImage. 2015;119:338–351.

48. Smith RE, Tournier J-D, Calamante F, Connelly A. Anatomically-constrained tractography: Improved diffusion MRI streamlines tractography through effective use of anatomical information. NeuroImage. 2012;62:1924–1938.

Case	Sex	Age	Extent of bilateral PVNH	Location of Nodules	*Filamin A* mutation	Epilepsy status
1	M	34	Sparse	Temporo-Occipital, Paratrigonal	Not tested	Affected
2	F	67	Sparse	Occipital, Paratrigonal	None	Affected
3	M	30	Sparse	Occipital, Frontal, Paratrigonal	None	Affected
4	M	39	Sparse	Temporal, Paratrigonal	None	Affected
5	F	34	Sparse	Temporal, Paratrigonal	None	Affected
6	F	18	Diffuse	Frontal, Parietal, Temporal, Occipital	None	Affected
7	M	34	Diffuse	Frontal, Parietal, Temporal, Occipital	None	Affected
8	F	43	Diffuse	Frontal, Parietal, Temporal, Occipital	c.6204insT	Affected
9 (Family A)	F	48	Diffuse	Frontal, Parietal, Temporal, Occipital	c.2751-2delGG	Unaffected
10 (Family A)	F	17	Diffuse	Frontal, Parietal, Temporal, Occipital	c.2751-2delGG	Affected
11	F	39	Diffuse	Frontal, Parietal, Temporal, Occipital	c.7103insA	Affected
12 (Family B)	F	35	Diffuse	Frontal, Parietal, Temporal, Occipital	c.1066-2 A>G*	Affected
13 (Family B)	F	68	Diffuse	Frontal, Parietal, Temporal, Occipital	c.1066-2 A>G*	Unaffected
14 (Family B)	F	0.3	Diffuse	Frontal, Parietal, Temporal, Occipital	c.1066-2 A>G*	Unaffected

Table 1: Patient demographic data, radiological description of PVNH and Epilepsy and *Filamin A* (*FLNA*) mutational status. *Details of mutation and clinical descriptions of members from family B, with the exception of the infant (patient 14), and functional MRI data from patient 11, have previously been published (3,23,24, and 12 respectively).

Figure Legends

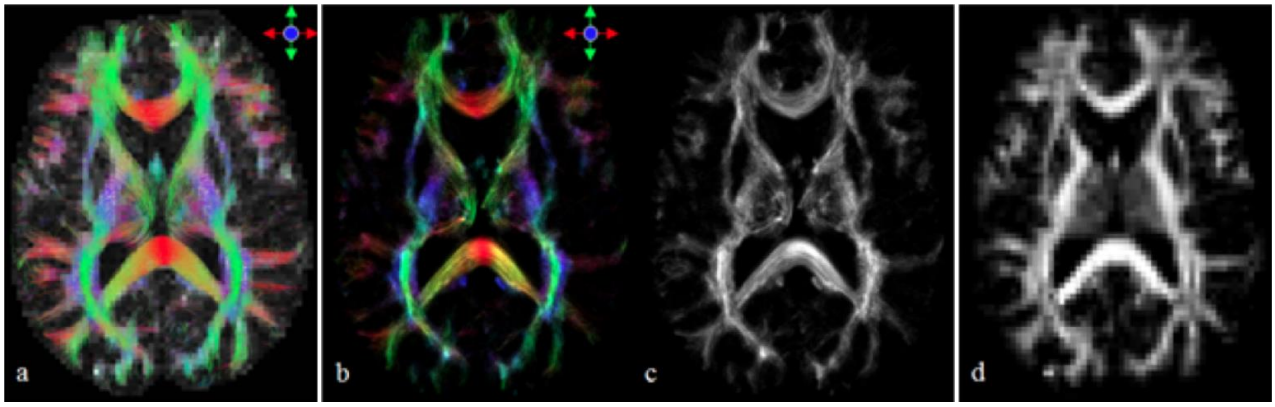

Figure 1: Axial images from a healthy control participant: **(a)** whole-brain fibre tractography, **(b-c)** whole brain super-resolution track density imaging (TDI) displayed as **(b)** a colour-coded DEC TDI map & **(c)** a TDI greyscale map, **(d)** the original fractional anisotropy (FA) map created at the acquired spatial resolution ($2.5mm^3$). Note the improved spatial detail available in regions such as the thalamus in images **(b & c)** compared to the original data resolution presented in image **(d)**. Images **(a-b)** are colour coded according to direction: red=left-right, green=anterior-posterior, blue=inferior-superior.

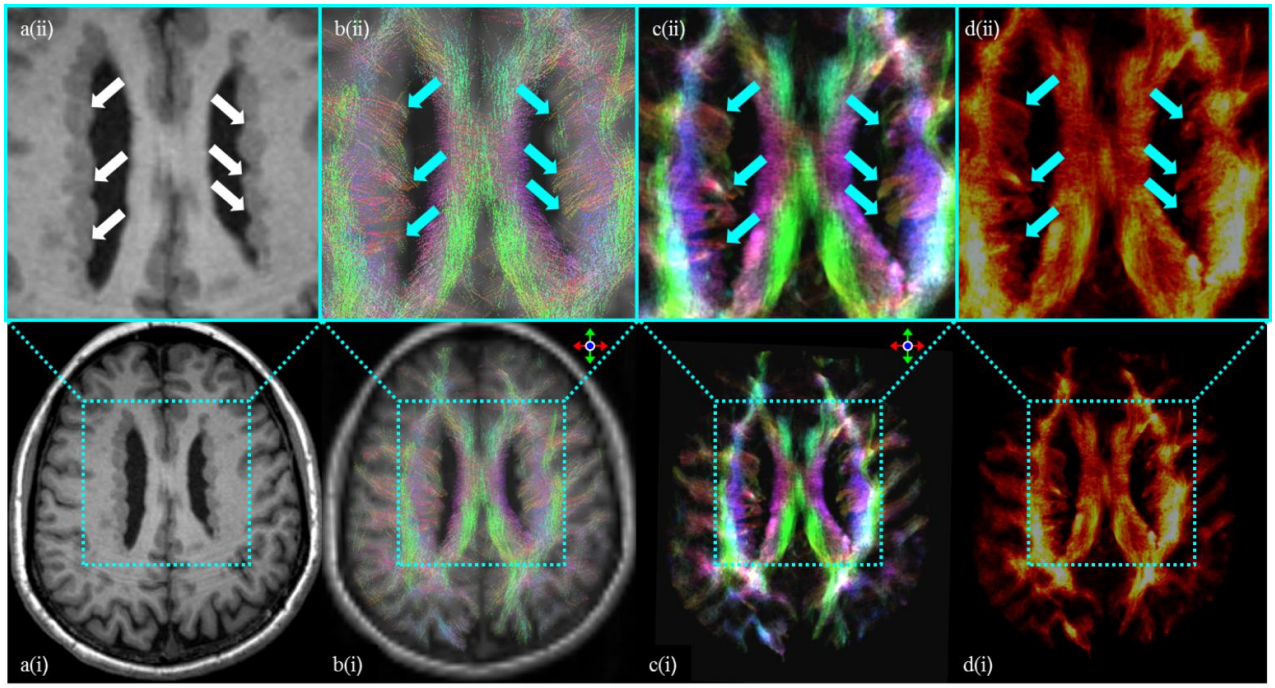

Figure 2: Axial images from an 48 year old female (Patient 9, *FLNA* positive) with diffuse bilateral PVNH (i), with magnified views (ii) of the regions indicated by the blue rectangles of **(a)** T1 weighted anatomical image, **(b)** whole-brain CSD-based tractography result, **(c-d)** whole-brain TDI maps derived from CSD-based tractography results super-resolved by applying a 500μm^3 grid. Images **(c)** are displayed as colour-coded DEC-TDI maps, and images **(d)** is the same TDI data with intensities displayed as a heat-scale. Images **(b-c)** are colour coded according to direction: red=left-right, green=anterior-posterior, blue=inferior-superior. Note the abnormal fibres projecting from some of the nodules lining the periventricular wall (images **(b-d)** blue arrows; white arrows on image **(a)** show the equivalent position anatomically).

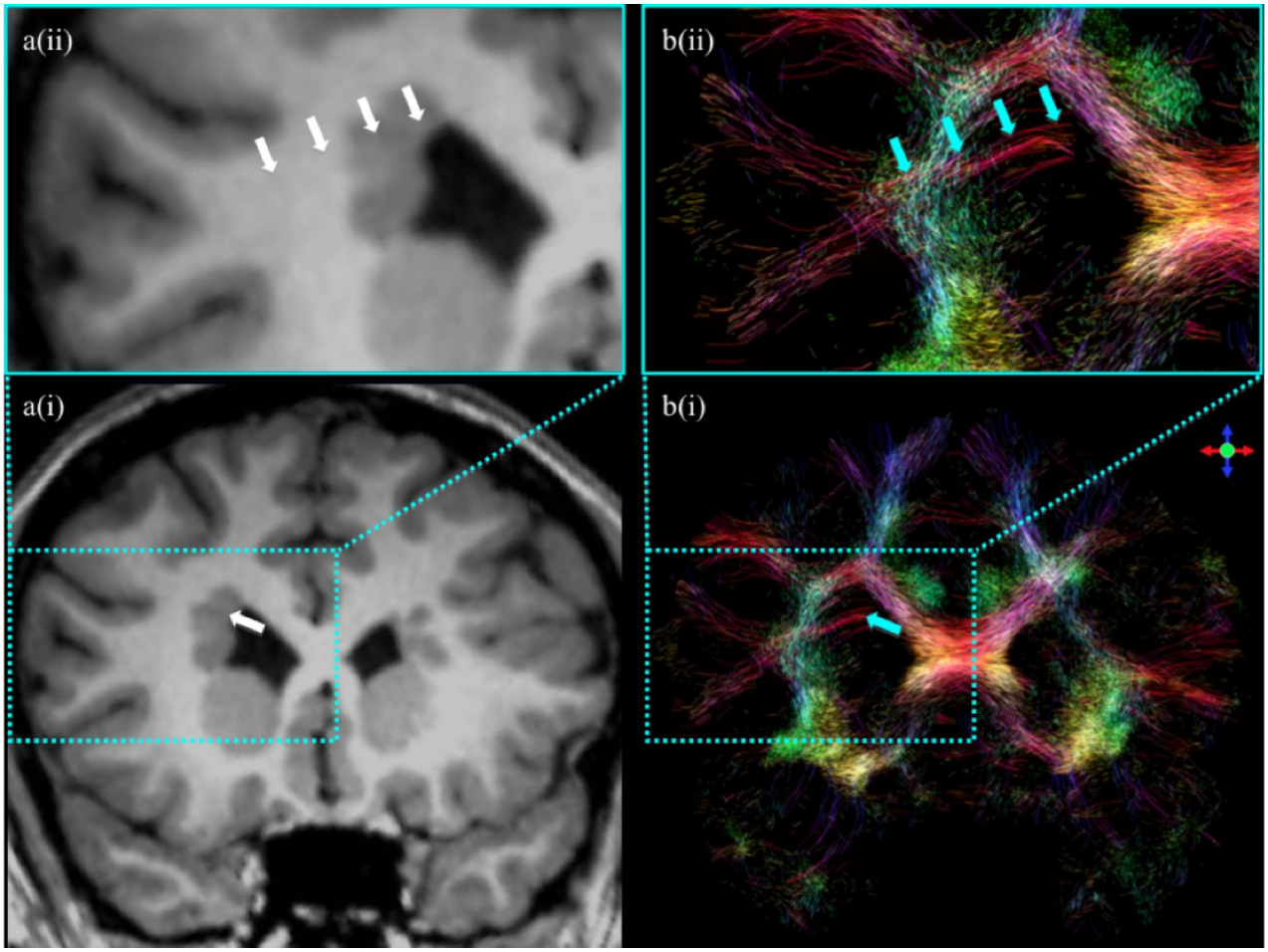

Figure 3: Coronal images (i) from an 18 year old female (patient 6, *FLNA* negative) with bilateral PVNH, with magnified views (ii) of the regions indicated by the blue rectangles showing **(a)** T1 weighted anatomical images, **(b)** corresponding whole brain CSD-based tractography results. Images **(a)** are colour coded according to direction: red=left-right, green=anterior-posterior, blue=inferior-superior. (Note the CSD-based fibre tractography streamlines technique depicts the path of abnormal fibre tracks (blue arrows) projecting laterally toward the cortex from within the right frontal nodule, (white arrows show the equivalent position anatomically on coronal anatomical T1 images (a)).

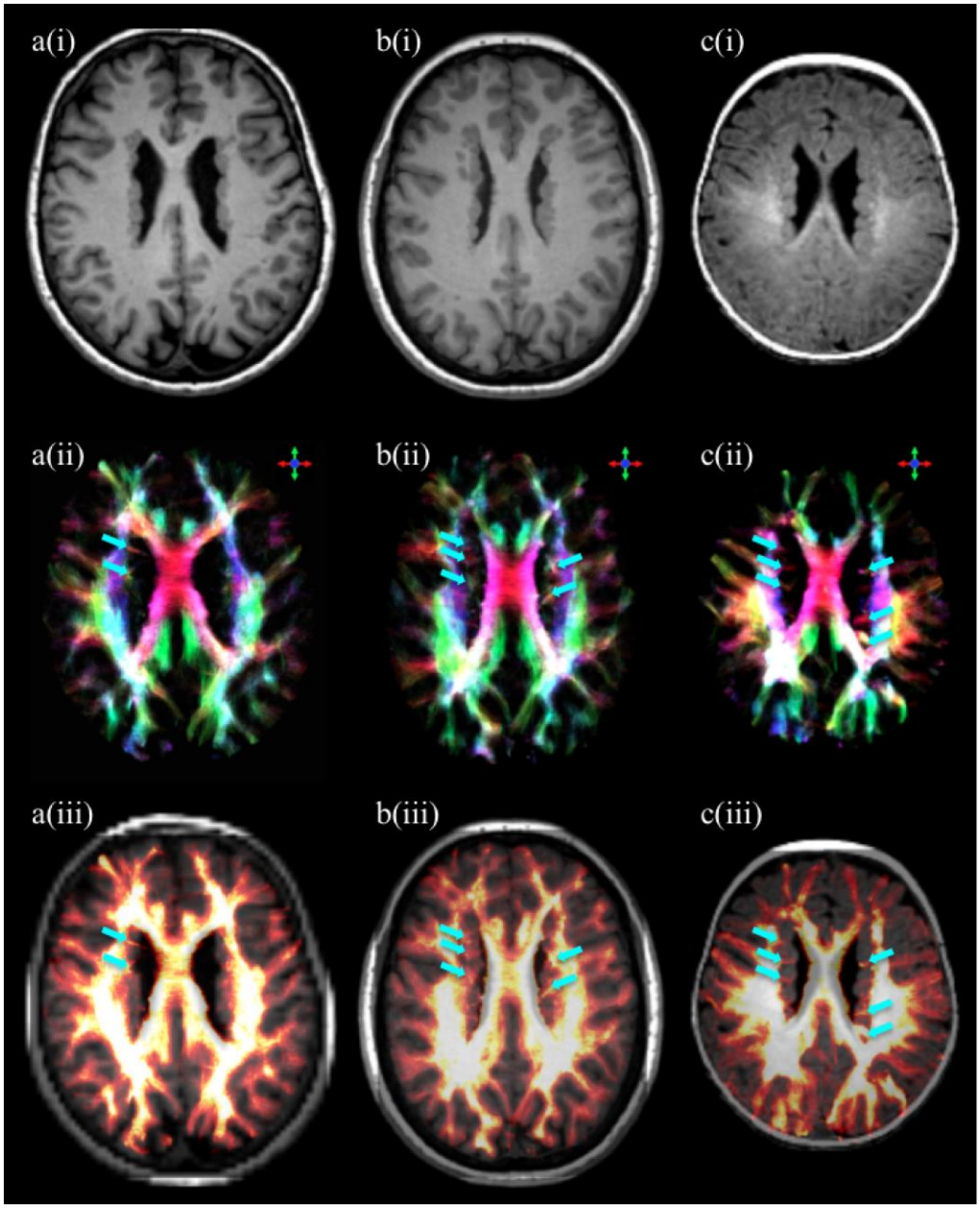

Figure 4: Axial images from 3 generations of a family with a *FLNA* mutation: **(a)** grandmother (68 years) (patient 13), **(b)** mother (35 years) (patient 12), and **(c)** daughter (4 months) (patient 14). Images **(a-c)**(i) T1 weighted anatomical images. Images **(a-c)** (ii)(iii) TDI maps derived from whole-brain CSD-based tractography results super-resolved by applying a 500μm^3 grid. Images (a-c)(ii) are DEC TDI maps with the local fibre orientations colour coded according to direction: red=left-right, green=anterior-posterior, blue=inferior-superior. Images **(a-c)**(iii) is the same TDI data with intensities displayed as a heat-scale, and overlaid on the T1 weighted anatomical images. Note the abnormal fibres projecting from some of the nodules lining the periventricular wall regions in all three patients (see regions identified by the blue arrows on images (ii-iii).

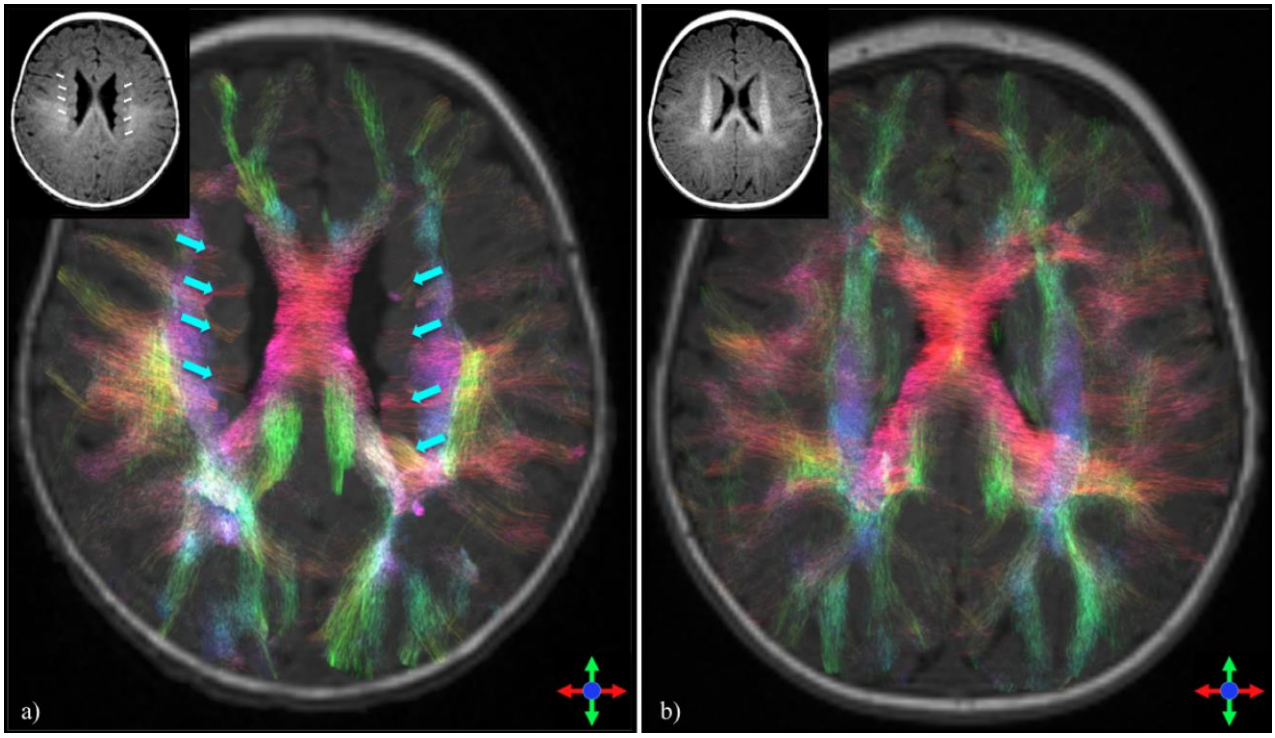

Figure 5: Whole-brain CSD-based tractography results overlaid on T1 weighted images from **(a) the 4 month old female with bilateral PVNH (*FLNA* positive; patient 14)** shown in Figure 4, and **(b) a 4 month old female healthy participant**. The corresponding axial T1 images are shown separately (inset top left) to demonstrate the anatomical location. The local fibre orientations are colour coded according to direction: red=left-right, green=anterior-posterior, blue=inferior-superior. Note the abnormal fibres projecting laterally from some, but not all, of the nodules lining the periventricular wall (blue arrows on tractography image (a); the white arrows (on the image inset top left) shows the equivalent anatomical location of these regions on the axial T1 image).

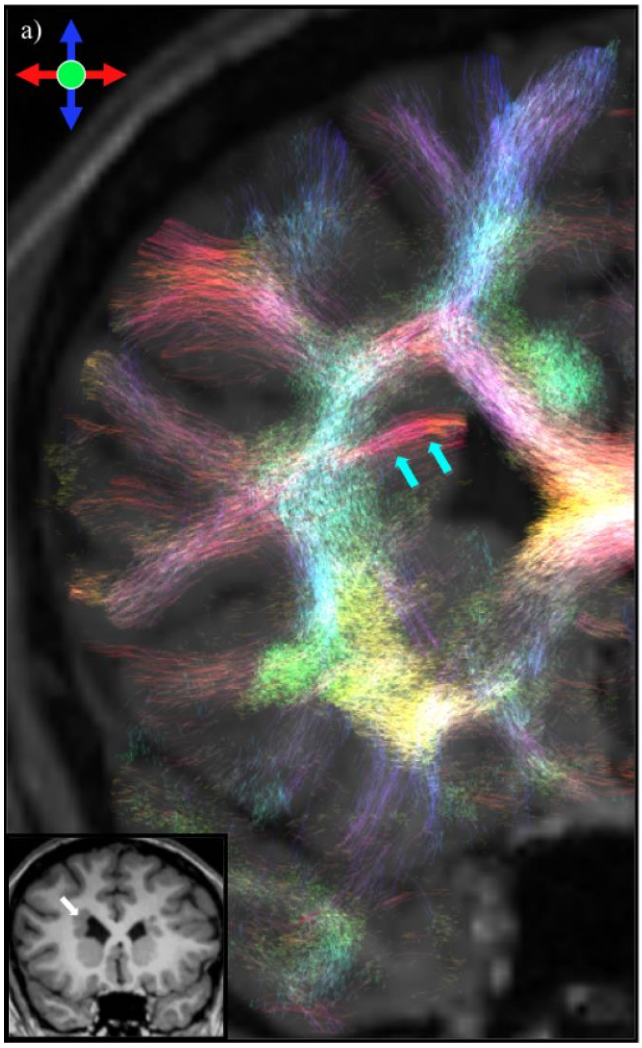

Image not available due to copyright restrictions

Figure 6: Histopathology results from Kakita et al. (9) - Coronal autopsy section of the right cerebral hemisphere demonstrating the histopathological features of a 48 year female with bilateral PVNH; confirmed with DiI tracing to have heterotopic nodules containing linear bundles of myelinated fibres within the nodule nest (black arrow), and a thin white matter bundle extending from the ventricular surface separating the nodule and the caudate nucleus (black arrow). Figure 6 is reprinted from Kakita et al., (2002). '*Bilateral periventricular nodular heterotopia due to Filamin 1 gene mutation: widespread glomeruloid microvascular anomaly and dysplastic cytoarchitecture in the cerebral cortex. Acta Neuropathol'*. (Berl.) (9), with kind permission from Springer Science and Business Media.